CRYSTAL GROWTH & DESIGN

pubs.acs.org/crystal

Article

Facilitating Nitrification Inhibition through Green, Mechanochemical Synthesis of a Novel Nitrapyrin Complex

Published as part of a Crystal Growth and Design virtual special issue in Celebration of the Career of Roger Davey

Lucia Casali, Valquiria Broll, Stefano Ciurli,* Franziska Emmerling,* Dario Braga, and Fabrizia Grepioni*

Cite This: *Cryst. Growth Des.* 2021, 21, 5792–5799

Read Online

ACCESS | Metrics & More | Article Recommendations | Supporting Information

ABSTRACT: Nitrapyrin (NP) is applied to cultivated soils to inhibit the enzymatic activity of ammonia monooxygenase (AMO), but its poor aqueous solubility and high volatility severely limit its application. β-Cyclodextrin (β-CD) is commonly used to form inclusion complexes with hydrophobic molecules, improving water solubility and stability upon complexation. Here we report on the mechanochemical synthesis of the inclusion complex β-CD·NP, characterized via a combination of solid-state techniques, including *ex-situ* and *in situ* X-ray diffraction, Raman and NMR spectroscopies, transmission electron microscopy, and energy dispersive X-ray spectroscopy. The pure inhibitor NP was also structurally characterized. The β-CD·NP complex presents improved solubility and thermal stability, and still inhibits the enzymatic activity of AMO with high efficacy. All results indicate that the inclusion of NP into β-CD represents a viable route for the preparation of a novel class of inhibitors, with improved properties related to stability, water solubility, and good inhibition activity.

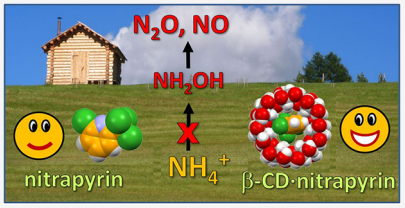

INTRODUCTION

With global agricultural production ever-expanding,[1] the quest for sustainable soil fertilization and crop productivity is all the more necessary.[2] Ending hunger, achieving food security, improving nutrition and promoting sustainable agriculture—as stated in the 2030 Agenda for Sustainable Development—represent real challenges of these times.[3,4] To the present day, approximately 50% of nitrogen (N) fertilizer applied to the soil is lost to the environment as greenhouse gases (NH_3, NO, and N_2O) or as leached NO_3^-, instead of being utilized by plants.[5] The N loss is mainly due to the activity of soil enzymes such as the nickel-dependent urease[6] and the copper-dependent enzyme ammonia monooxygenase (AMO),[7] the latter initiating the nitrification process by catalyzing the oxidation of unassimilated ammonium (NH_4^+) into hydroxylamine (NH_2OH).[8] AMO is produced by ammonia oxidizing bacteria (AOB) along with the enzymes hydroxylamine oxidoreductase (HAO) and nitric oxide reductase (NOR), which complete the nitrification process.[9] HAO catalyzes the conversion of NH_2OH into nitrite (NO_2^-), which is then transformed to gaseous forms of N such as nitric oxide (NO) and nitrous oxide (N_2O). When nitrite is not involved in these processes, it is converted by NOR into nitrate (NO_3^-), which can be taken up by plant roots, leached into groundwater, or become involved in the anaerobic denitrification route.[10]

Given the negative economic, agronomic, and environmental consequences arising from the nitrification process, the current agrochemical formulations are aimed to increase N use efficiency by using inhibitors of urease and AMO.[11,12] Several inhibitors impact the first step of nitrification, with AMO being the enzyme target.[13−15]

However, the search for AMO inhibitors is complicated by the difficulty to obtain the enzyme in a fully functional form unless intact cells of AOB are used. The scarce information concerning the chemical structure of AMO has only recently been complemented with models built by taking advantage of the similarity between AMO and particulate methane monooxygenase (pMMO) from a catalytic, structural, and genetic point of view.[16] In particular, the latter study supports a model for the enzyme in which the active site contains a Cu(II)/(I) ion coordinated by two histidine imidazole N atoms and one aspartate carboxylic O atom, featuring a labile water molecule that completes a pseudo-tetrahedral ligand geometry in the so-called CuC site (Scheme 1).[16]

Nitrapyrin (NP, 2-chloro-6-(trichloromethyl) pyridine) (Scheme 1) is a very effective inhibitor of AMO, acting in the nM range.[17a] The mechanism by which NP inhibits nitrification has been proposed to involve the AMO-catalyzed oxidation of NP to 6-chloropicolinic acid (6-CPA), with the

Received: June 14, 2021
Published: September 13, 2021

https://doi.org/10.1021/acs.cgd.1c00681
Cryst. Growth Des. 2021, 21, 5792−5799

Scheme 1. Representation of the CuC Center in the Active Site of AMO (A), the Inhibitor Nitrapyrin (NP, 2-Chloro-6-(trichloromethyl)pyridine) (B), and β-Cyclodextrin (β-CD) (C)

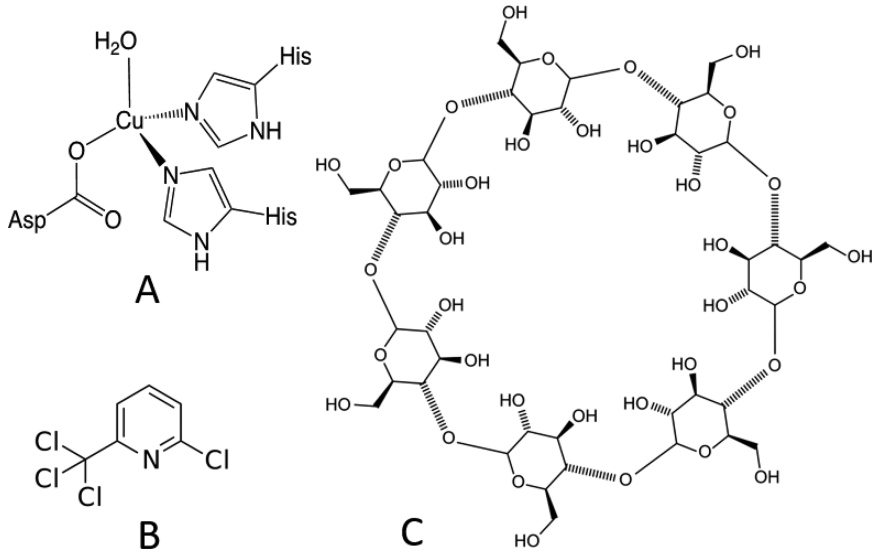

latter binding nonspecifically to other membrane proteins, thus critically affecting the electron transfer chain.[17b] However, previous studies contrast with this hypothesis.[17c] Experiments of AMO inhibition by 6-CPA, carried out in our laboratories (not shown), showed only a 40% reduction of enzymatic activity at 1 mM concentration, a result supporting the noncompetence of 6-CPA as a nitrification inhibitor. The direct interaction of NP with the Cu(II)/Cu(I) ion in the CuC-containing active site of AMO is a possibility that cannot be ruled out.

The high efficacy of NP as a nitrification inhibitor is accompanied by its high vapor pressure, a characteristic that induces its incorporation into the soil via injection at a depth of at least 5−10 cm and preferably in cold-climate countries;[18] alternatively, a microcapsules formulation has been patented and commercialized to reduce losses and improve release into the soil.[19] In addition to this, NP presents an extremely low water solubility, as well as some safety issues, which limit its use and potential.[20]

In the past few years, we have succeeded in improving physicochemical properties of urease and AMO inhibitors via cocrystallization with organic molecules and inorganic salts.[21−23] In this work, we report on a successful attempt to improve the properties of NP through mechanochemical cocrystallization with β-cyclodextrin.

β-Cyclodextrin (β-CD, see Scheme 1) belongs to the family of cyclodextrins, cyclic oligosaccharides with glucose units—6 (α-cyclodextrins), 7 (β-cyclodextrins), or 8 (γ-cyclodextrins)—bonded via α-1,4 glycosidic bonds;[24] all cyclodextrins possess a hydrophobic cavity—able to include apolar guests—and a hydrophilic surface, which makes the resulting inclusion compounds soluble in water. Through the preparation of β-CD inclusion complexes it is generally then possible to (i) improve the water solubility/stability of the guest molecules, (ii) perform a controlled release of the included molecules, and (iii) increase the bio- and ecocompatibility of the guest molecules.[25] As a result of these properties, β-CD has been widely employed as a drug carrier in the pharmaceutical field,[26] as well as in the food industry and in the environmental sciences.[27,28] Interestingly, although the preparation of β-CD inclusion complexes with agrochemicals has been reported,[29−32] there are no studies concerning the stabilization of AMO inhibitors by inclusion into the β-CD cavity. β-CD is relatively safe to humans and to the environment, and is not expensive.

Here we describe the synthesis of the inclusion complex β-CD·NP, performed via mechanochemical reaction of NP and β-CD in a 1:1 stoichiometric ratio in the presence of a minimum amount of water. The crystalline solid obtained was characterized by X-ray diffraction, Raman and NMR spectroscopies, TEM/EDX, and thermogravimetric analysis. A full solid-state characterization of pure NP was also conducted. The improved solubility properties of β-CD·NP in water allowed us to establish its efficacy as an AMO inhibitor in *Nitrosomonas europaea* cell cultures. These results represent a significant step toward the utilization of β-CD·NP to enhance the efficiency of nitrogen soil fertilization.

EXPERIMENTAL SECTION

Materials and Instrumentation. All reagents were purchased from Sigma-Aldrich and used without further purification. *Nitrosomonas europaea* (*N. europaea*, ATCC 19718) was purchased from ATCC (Manassas, USA).

Mechanochemical Synthesis. The inclusion complex β-CD·NP was obtained by ball milling, using a Retsch Mixer Mill MM 400, β-CD·8H_2O (67.76 mg, 0.052 mmol), and NP (12.24 mg, 0.052 mmol), with the addition of 80 μL (0.044 mmol) of water, for 120 min at 20 Hz in an agate jar. Larger quantities of water (up to 120 μL, 0.066 mmol) yielded the same product (see Supporting Information for details on phase identification of the product by X-ray powder diffraction). For the *in situ* synchrotron X-ray diffraction measurements, the synthesis was performed using a vibration ball mill (Pulverisette 23, Fritsch, Idar-Oberstein, Germany). The materials were kneaded, with the addition of 80 μL of water, in a PMMA jar with two 5 mm stainless steel milling balls at 50 Hz.

Single-Crystal X-ray Diffraction. Single-crystal data on pure NP single crystals, grown from an ethanol solution, were collected at RT with an Oxford XCalibur S CCD diffractometer equipped with a graphite monochromator (Mo−Kα radiation, λ = 0.71073 Å). The structure was solved by intrinsic phasing with SHELXT5[33] and refined on F2 by full-matrix least-squares refinement with SHELXL[34] implemented in the Olex2 software. All non-hydrogen atoms were refined anisotropically. The program Mercury[35] was used to calculate

https://doi.org/10.1021/acs.cgd.1c00681
Cryst. Growth Des. 2021, 21, 5792−5799

the powder patterns from single-crystal data and for molecular graphics. See Table S1 for crystal data and details of measurement. Crystal data can be obtained free of charge via www.ccdc.cam.ac.uk/conts/retrieving.html (or from the Cambridge Crystallographic Data Centre, 12 Union Road, Cambridge CB21EZ, UK; fax: (+44) 1223-336-033; or e-mail: deposit@ccdc.cam.ac.uk). CCDC 2074290.

Powder X-ray Diffraction (PXRD). For phase identification (Figure S1), PXRD patterns of β-CD·NP and starting material were collected in Bragg−Brentano geometry on a PANalytical XPert Pro Automated diffractometer, equipped with an Xcelerator detector, using Cu−Kα radiation (λ = 1.5418 Å) without a monochromator in the 5−50° 2θ range (step size 0.033°; time/step: 20 s; soller-slit 0.04 rad, antiscatter slit: 1/2, divergence slit: 1/4; 40 mA, 40 kV). For Pawley refinement (Figure S2), PXRD patterns were collected in transmission geometry on a PANalytical X'Pert PRO automated diffractometer, equipped with a focusing mirror and pixel detector, in the 3−70° 2θ range (step size 0.02608, time/step 200 s, 0.02 rad soller; 40 kV, 40 mA). Powder diffraction data were analyzed with the software TOPAS4.1.[36] A shifted Chebyshev function with six parameters was used to fit the background.

***In Situ* Powder X-ray Diffraction.** *In situ* measurements were performed every 30 s at the μSpot beamline (BESSY II, Helmholtz Centre Berlin for Materials and Energy) on β-CD (50.82 mg) and NP (9.17 mg) ball-milled in a PMMA jar at 50 Hz. The experiments were conducted with a wavelength of 1 Å using a double crystal monochromator (Si 111).[37] The resulting X-ray diffraction patterns were processed with the software DPDAK[38] and the background corrected.

Raman Spectroscopy. Raman spectra were recorded on β-CD, NP, and β-CD·NP by using a LabRam HR 800 instrument (Horiba Jobin Yvon) coupled to a BX41 microscope (Olympus). The system is equipped with a diode-pumped solid-state (DPSS) laser that has a wavelength of 532 nm and 300 mm^{-1} grating. The laser power was reduced by neutral density filters to 10% of the full laser output power to avoid laser damage. All spectra were acquired with 10 s accumulation time and 50 times magnification. Before the Raman measurements were performed, the laser was allowed to stabilize for at least 2 h, and the spectrometer was recalibrated against the most prominent mode of silicon at 520.7 cm^{-1}.

TEM Characterization. Transmission electron microscopy (TEM) images were obtained with a Talos F200S microscope (Thermo Fisher Scientific) using an accelerating voltage of the electron beam of 200 kV. The β-CD·NP powders were dispersed in water (~2 mg mL^{-1}), deposited in carbon−Formvar-coated Cu grids, and dried in air. To determine the elemental composition of the sample, energy dispersive X-ray spectroscopy (EDX) with two silicon drift detectors (SDD) was used during TEM analysis (dwell time = 20 μs).

^{1}H NMR Spectroscopy. β-CD·NP powder was dissolved in D_2O, and ^{1}H NMR spectra were recorded on a Varian INOVA 400 (400 MHz) spectrometer. Chemical shifts are reported in ppm, with tetramethylsilane as an internal reference standard.

Thermogravimetric Analysis (TGA0. TGA measurements were performed with a PerkinElmer TGA7 thermogravimetric analyzer, under an N_2 gas flow and at a heating rate of 5.00 °C min^{-1}, in the 30−175, 30−450, and 30−350 °C temperature ranges for NP, β-CD, and β-CD·NP, respectively.

Ammonia Monooxygenase Enzymatic Inhibition by NP and β-CD·NP. Bacterial cell growth. *N. europaea* cells were grown as previously described.[23] Briefly, cells where grown in 1.5 L of ATCC2265 medium, in the dark at 26 °C. After 72 h, cells were harvested by centrifugation at 14000*g* for 20 min at 4 °C, washed with a 100 mM sodium phosphate buffer at pH 7.5, also containing 2 mM $MgSO_4$ (NaPB buffer), resuspended in 6 mL of the same buffer, and quantified by their total protein content using the biuret assay.[39] Stock solutions (aliquots of ca. 0.5 mL) with a total protein concentration of ca. 2.5 mg mL^{-1} were prepared.

***Nitrosomonas europaea* AMO Activity Measurement by O_2 Consumption.** Consumption of dioxygen (O_2) was determined using a Clark-type polarographic electrode (Vernier, Oregon, USA) and a LabQuest2 sensor data collection system (Vernier, Oregon, USA), as previously described.[23] The experiment was initiated by adding one aliquot of *N. europaea* cells to NaPB buffer at pH 7.5 containing 10 mM $(NH_4)_2SO_4$ (5 mL final volume, providing a total protein content of ca. 0.5 mg) after a 3 min pre-equilibration period to establish a baseline for the measurement. The traces of recorded O_2 concentration versus time were followed for 20 min and integrated over time to obtain the total amount of O_2 consumed by *N. europaea* in this time. For the integration procedure, the trace describing the O_2 concentration versus time in the absence of substrate was used as the baseline. Experiments using either β-CD or DMSO were carried out as a control. A stock NP solution was prepared by first solubilizing the compound in 100% DMSO; the latter solution was used to prepare NP work solutions in NaPB buffer, containing <0.2% (v/v) final concentration of DMSO. Solutions of the β-CD·NP adduct were prepared by adding the solid material to NaPB buffer in the absence of DMSO, and both compounds were tested at a final concentration of 100 μM. The same analysis was performed after a 2 h incubation between NP or β-CD·NP with the same quantity of cells tested before. The incubation was carried out at 26 °C, in the dark and with constant stirring. The reaction, in these cases, was started by $(NH_4)_2SO_4$ addition. All experiments were conducted in triplicates as independent experiments, in the dark and under constant stirring. Measurements were normalized with respect to the O_2 consumption measured in the reference experiment and plotted as a percentage; the data were expressed as mean ± standard deviation (SD).

***Nitrosomonas europaea* AMO Activity Measurement by Nitrite Production.** The protocol was carried out as previously described.[23] *N. europaea* cells produce nitrite (NO_2^-) as the nitrification product, which was spectrophotometrically determined by the Griess test[40] using a Cary 60 UV−vis spectrophotometer (Agilent, CA, USA). Nitrite production by *N. europaea* was started upon addition of one aliquot of cells in the reaction mixture (5 mL final volume, providing a total protein content of ca. 0.5 mg) composed by NaPB buffer, 50 μM $(NH_4)_2SO_4$ as substrate and in the absence (control experiment) or presence of NP or β-CD·NP at a final concentration of 100 μM. After a 60 min incubation, the colorimetric reaction was started by treating for 30 min with the Griess reagent followed by measurements of the absorbance at 548 nm. The same nitrite production experiments were conducted following a prior incubation between *N. europaea* cells and NP or β-CD·NP in the same buffer mixture at inhibitor concentrations from 0 to 100 μM for 2 h, at 26 °C, in the dark and constant stirring. All measurements were normalized with respect to the amount of nitrite produced in the reference experiment and plotted, as a percentage, as a function of the amount of the NP or β-CD·NP, and the data were expressed as mean ± standard deviation (SD). A control experiment was carried out using a reaction mixture composed of 50 μM $(NH_4)_2SO_4$ in NaPB buffer incubated for 60 min with either NP or β-CD·NP, in the dark at room temperature, to exclude interference at 548 nm. All experiments were conducted in triplicates as independent experiments, in the dark, at 25 °C and under constant stirring.

RESULTS AND DISCUSSION

The first step in this study was the characterization of the solid-state properties of pure NP; to this goal, single crystals of NP suitable for X-ray diffraction (see Supporting Information) were grown from an ethanol solution. Layers of nitrapyrin molecules are stacked in their crystal (Figure 1), with aromatic planes at close contact (average interplanar distance 3.604(5) Å).

The nitrogen atom does not act as a Lewis base or a nucleophile, and an approach to its position is sterically hindered by the large $-CCl_3$ group, which in the solid state is oriented in the most favorable conformation for the π-stacking arrangement. As a result, cocrystallization—for example, with urease inhibitors as quinones[41]—and salification attempts, both in solution and in the solid state, were unsuccessful.

https://doi.org/10.1021/acs.cgd.1c00681
Cryst. Growth Des. 2021, 21, 5792−5799

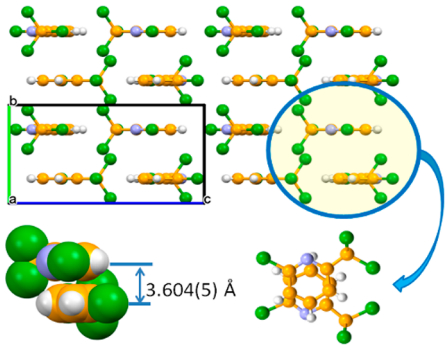

Figure 1. $\pi-\pi$ stacking of NP molecules along the *b*-axis direction (top) and the average distance between adjacent aromatic planes (bottom left); projection of two molecules along the stack, showing the staggered arrangement of the $-CCl_3$ groups (bottom right). Chlorine, carbon, and nitrogen atoms in green, orange, and light blue, respectively.

Given the marked hydrophobicity of NP, we decided to test its reactivity with β-CD[24] (Scheme 1), whose cavity size was expected to be large enough to accommodate the nitrapyrin molecule.

Preliminary attempts to form a complex from solution synthesis were unsuccessful; therefore, we focused our attention on the preparation of the inclusion complex via mechanochemistry.[42,43] To this end, β-CD and NP were kneaded together for 2 h in a 1:1 stoichiometric ratio in the presence of an almost equimolar amount of water (see Supporting Information); grinding in dry conditions invariably resulted in a physical mixture of the reagents.

The time course of the mechanochemical reaction was determined through X-ray diffraction in situ measurements (Figure 2).[44] In particular, the variation in the intensity of the

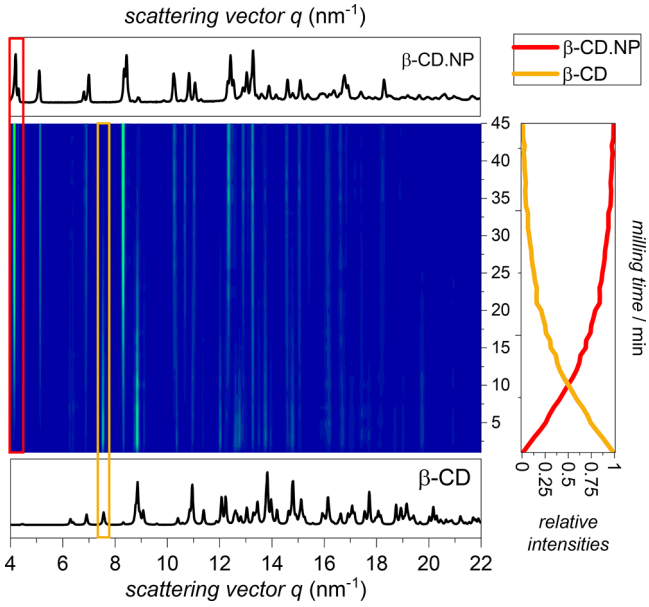

Figure 2. 2D plot of the diffractograms recorded with synchrotron radiation during the mechanochemical reaction between β-CD and NP. One reflection from β-CD and one from β-CD·NP, evidenced by yellow and red lines, respectively, on the left part of the figure, were followed over a 45 min time interval; the relative intensities versus time are plotted on the right-hand side box.

reflection from the *hkl* plane of β-CD at 7.53 nm^{-1} (yellow line) and that of β-CD·NP at 5.11 nm^{-1} (red line) was monitored, over a 45 min time interval, thus obtaining information on the kinetics of complexation. As evidenced in Figure 2, the complex begins forming in the first few minutes, and the reaction is complete after 45 min, as confirmed by the absence of reflections for β-CD.

The principle of isostructurality pointed out in Caira's work[45] was employed in order to describe the possible arrangement of the β-CD molecules in crystalline β-CD·NP. β-CD molecules crystallize in eight possible isostructural series, and, according to Caira's principle, within each series the β-CD molecules are arranged essentially in the same fashion, with close unit cell parameters. As a consequence, the PXRD patterns within the same isostructural series are extremely similar and fairly superimposable, regardless of the chemical nature of the guest molecules.[30] A Pawley refinement (Figure S2) on the experimental pattern proved that it matches well with the isostructural series characterized by the channel-type packing of β-CD dimers in the monoclinic space group *C*2,[46,47] usually adopted in the presence of medium/large guest molecules (see Figure 3a); a graphical representation of a

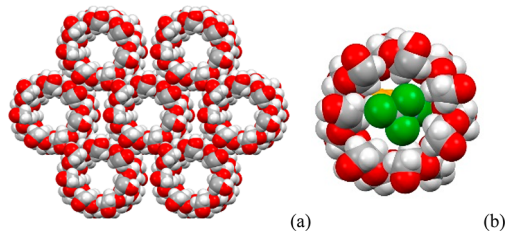

Figure 3. (a) The channel-like packing of β-CD molecules typically observed within the isostructural series C2.[47] (b) Graphical representation of a possible arrangement (obtained via the program Mercury[35]) of the NP molecule within the hydrophobic cavity of a β-CD molecule. Carbon atoms of β-CD and NP are in gray and orange, respectively; oxygen atoms are in red.

possible arrangement of the NP molecule inside the β-CD hydrophobic cavity is shown in Figure 3b.[35] On the contrary, when the β-CD cavities contain only water molecules, as in the starting hydrate, crystallization in the monoclinic $P2_1$ space group is invariably observed.

The β-CD·NP complex was also characterized by Raman measurements performed on the crystalline powder product obtained via mechanochemical synthesis. Despite the large number of covalent bonds present in β-CD, the active Raman modes are limited, due to the low polarizability of the molecule, while the aromatic ring of the NP molecule is strongly Raman active, thus making the inclusion of NP into β-CD readily detectable.[48,49] Figure 4 reports a comparison of the Raman spectra for β-CD·NP, β-CD, and NP in the range 3300−400 cm^{-1}. Bands of both components can be observed in the spectrum of the inclusion compound, but they are shifted in wavenumber position and changed in relative intensity and spectral profile with respect to pure components, as evidence of the effective inclusion of NP into the β-CD cavity (see Supporting Information for details).[50] β-CD·NP presents a low crystallinity, as already observed for other β-CD inclusion complexes.[51]

Crystalline powder of β-CD·NP, as obtained by mechanochemical synthesis, was then suspended in water and analyzed through a combination of TEM/EDX techniques

https://doi.org/10.1021/acs.cgd.1c00681
Cryst. Growth Des. 2021, 21, 5792−5799

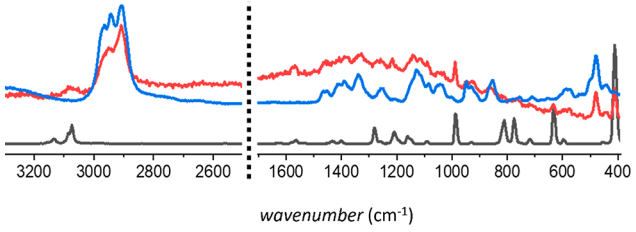

Figure 4. Comparison of the Raman spectra for β-CD·NP (red line), β-CD (blue line), and NP (black line) in the range 3330−400 cm^{-1} (the range 2600−1600 cm^{-1} is not reported, as no signals are present).

for its morphological characterization. As shown in Figure 5, β-CD·NP crystals are characterized by a rhombic shape, already

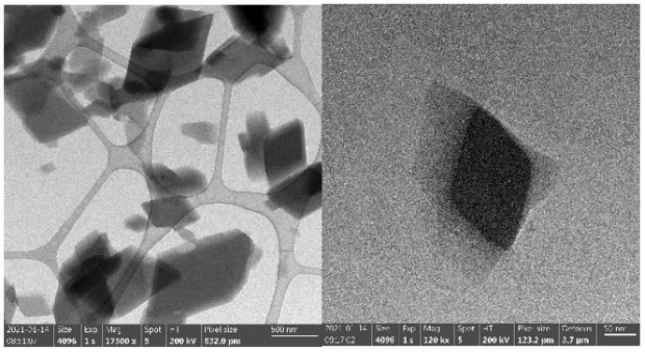

Figure 5. TEM images on the dispersed powders (left) and zoom on a single crystal (right).

observed in TEM mode for crystals of β-CD and β-CD inclusion compounds.[52−54] An EDX analysis was performed on a single crystal: the elemental analysis confirmed the presence of the expected chemical elements (Figure S4).

The stoichiometry of the β-CD·NP inclusion complex was assessed in solution via NMR spectroscopy in D_2O (Figure S5). The ^1H NMR chemical shifts of NP and β-CD fall into different regions; therefore, it was possible to detect the signals of NP despite the large contribution from β-CD. The stoichiometry of the complex, determined with good accuracy by exploiting the intrinsic quantitative character of NMR spectroscopy, was found to be 1:1 (Figure S5). The result is also consistent with literature data, as inclusion complexes in the isostructural C2 series are usually characterized by a 1:1 host/guest molar ratio.[55]

TGA measurements (see Supporting Information) were conducted on the reagents β-CD and NP as well as on the β-CD·NP complex. The thermal stability of NP, which as a pure substance melts in the 60−66 °C range and boils at 136 °C (P = 1 atm), is enhanced by more than 100 °C upon inclusion in β-CD, as major weight loss is observed starting only at ca. 200 °C (see Figure S6). The weight loss observed below 100 °C is due to the release of ca. three water molecules per formula unit (Figure S6).

The solubility of β-CD·NP in water at 20 °C is about 7.0×10^{-4} mol L^{-1} (1 g L^{-1}), while literature values for pure NP range between 8.7×10^{-5} and 17.3×10^{-5} mol L^{-1} (0.02−0.04 g L^{-1}):[56] significantly, an almost 10-fold increase in the water solubility of NP is thus observed upon complexation with β-CD.

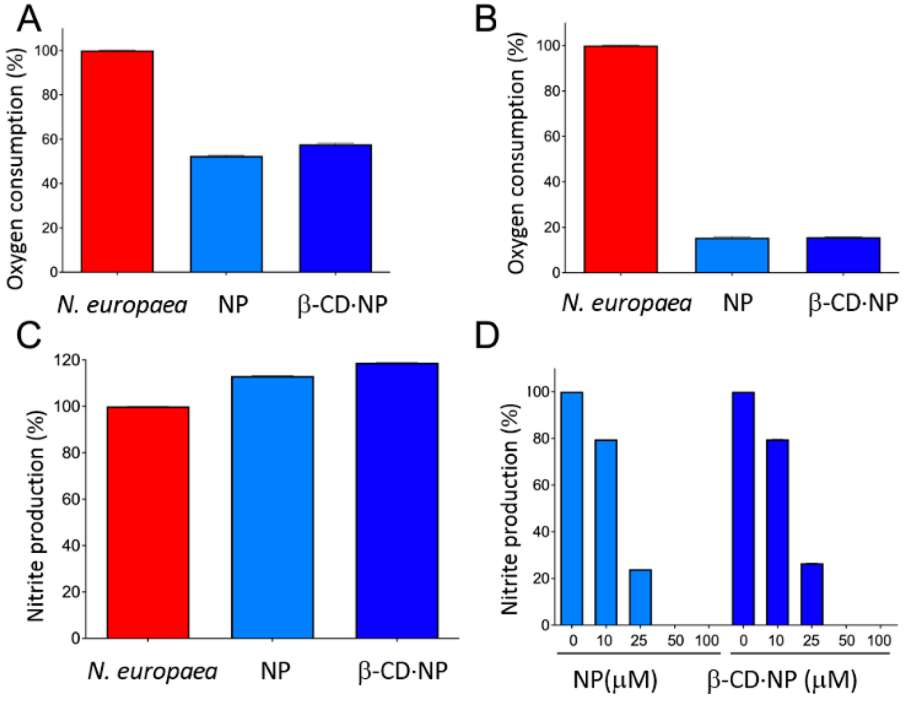

Figure 6. *Nitrosomonas europaea* nitrification activity. (A) O_2 consumption by *N. europaea* in the absence of inhibitors (red bar), in the presence of 100 μM NP (azure bar), or in the presence of 100 μM β-CD·NP complex (blue bar). (B) Oxygen consumption after 2 h incubation of *N. europaea* in the absence of inhibitors (red bar), in the presence of 100 μM NP (azure bar), or in the presence of 100 μM β-CD·NP complex (blue bar). (C) Nitrite production by *N. europaea* in the absence of inhibitors (red bar), in the presence of 100 μM NP (azure bar), or in the presence of 100 μM β-CD·NP complex (blue bar). (D) Nitrite production after 2 h incubation of *N. europaea* with an increasing amount of NP, from 0 to 100 μM (azure bar) or 2 h incubation with an increasing amount of β-CD·NP complex from 0 to 100 μM (blue bar). All experiments were performed in triplicate, and the data are expressed as mean ± SD (see Table S3).

https://doi.org/10.1021/acs.cgd.1c00681
Cryst. Growth Des. 2021, 21, 5792−5799

Both NP and β-CD·NP showed inhibition of *N. europaea* O_2 consumption by ca. 50% in the 20 min measurement time (Figure 6A). If *N. europaea* cells are preincubated in the presence of 100 μM NP or β-CD·NP for 2 h, a significant increase of the inhibition is observed for both compounds (Figure 6B). The inhibitory activity observed for both tested compounds is exclusively related to NP and not induced by either DMSO or β-CD. Nitrite (NO_2^-) production by *N. europaea* cells in the presence of 100 μM of NP or β-CD·NP in the absence of preincubation was spectrophotometrically determined using the Griess reaction. The nitrite production in the presence or absence of the tested compounds was all ca. 100% (Figure 6C). On the other hand, incubation of *N. europaea* cells with NP or β-CD·NP for 2 h causes the occurrence of an evident inhibition of NO_2^- production, in a concentration-dependent mode (Figure 6D).

CONCLUSIONS

We have reported here the preparation and full characterization of an inclusion complex between β-CD and nitrapyrin (NP) that is active against the soil enzyme ammonia monooxygenase (AMO). This study is a part of our ongoing efforts to employ crystal engineering strategies to produce more sustainable and more efficacious alternatives to agrochemicals currently used to tackle the problem of fertilizer degradation by soil enzymes.[21−23] The novel material permits us to fully exploit the inhibition activity of NP toward AMO by forming an inclusion complex with β-CD by a simple, cheap, high-yield, and environmentally friendly mechanochemical method.[42] The product has been characterized through a combination of *in situ* and *ex-situ* X-ray diffraction measurements, Raman and NMR spectroscopies, as well as TEM/EDX techniques. Thermogravimetric analysis and solubility tests show that the thermal stability and water solubility of NP are greatly enhanced upon complex formation. The pure inhibitor NP was also structurally characterized, as no information concerning its solid-state features was previously available. Finally, tests on the inhibition activity of both NP and β-CD·NP toward AMO proved that the inhibitory activity of NP is not altered upon inclusion in β-CD.

To the best of the authors' knowledge, the complex β-CD·NP represents not only the first stoichiometric complex of NP but also an extremely viable route for its stabilization, which may increase and facilitate its application as an AMO inhibitor. The green synthetic procedure (mechanochemical reaction in the presence of water), the improved handling, water solubility and thermal stability, and the efficacious inhibition activity of NP upon complexation can all be expected to have a significant impact on the nitrification process and its environmental consequences.

ASSOCIATED CONTENT

Supporting Information

The Supporting Information is available free of charge at https://pubs.acs.org/doi/10.1021/acs.cgd.1c00681.

Single-crystal and powder X-ray diffraction, Raman spectra, inhibition tests, TEM/EDX, solution NMR, TGA (PDF)

Accession Codes

CCDC 2074290 contains the supplementary crystallographic data for this paper. These data can be obtained free of charge via www.ccdc.cam.ac.uk/data_request/cif, or by emailing data_request@ccdc.cam.ac.uk, or by contacting The Cambridge Crystallographic Data Centre, 12 Union Road, Cambridge CB2 1EZ, UK; fax: +44 1223 336033.

AUTHOR INFORMATION

Corresponding Authors

Fabrizia Grepioni − *Department of Chemistry "G. Ciamician", University of Bologna, 40126 Bologna, Italy;* orcid.org/0000-0003-3895-0979; Email: fabrizia.grepioni@unibo.it

Stefano Ciurli − *Laboratory of Bioinorganic Chemistry, Department of Pharmacy and Biotechnology, University of Bologna, 40127 Bologna, Italy;* orcid.org/0000-0001-9557-926X; Email: stefano.ciurli@unibo.it

Franziska Emmerling − *BAM Federal Institute for Materials Research and Testing, 12489 Berlin, Germany;* orcid.org/0000-0001-8528-0301; Email: franziska.emmerling@bam.de

Authors

Lucia Casali − *Department of Chemistry "G. Ciamician", University of Bologna, 40126 Bologna, Italy*

Valquiria Broll − *Laboratory of Bioinorganic Chemistry, Department of Pharmacy and Biotechnology, University of Bologna, 40127 Bologna, Italy*

Dario Braga − *Department of Chemistry "G. Ciamician", University of Bologna, 40126 Bologna, Italy;* orcid.org/0000-0003-4162-4779

Complete contact information is available at: https://pubs.acs.org/10.1021/acs.cgd.1c00681

Notes

The authors declare no competing financial interest.

ACKNOWLEDGMENTS

We acknowledge financial support from the University of Bologna (F.G., D.B., S.C.), the Consorzio Interuniversitario di Risonanze Magnetiche di Metallo-Proteine (CIRMMP) (S.C., V.B.), and the Chemistry Department "G. Ciamician" (L.C., Marco Polo grant). We thank Dr. Stefano Grilli for his help with NMR measurements, Dr. Julien Marquardt for the acquisition of the Raman data and Dr. Carsten Prinz for his help with TEM analysis.

REFERENCES

(1) Evans, A. *The Feeding of the Nine Billion: Global Food Security for the 21st Century*; Chatham House Report. Chatham House: London, 2009; pp 1−59.

(2) Prosekov, A. Y.; Ivanova, S. A. Food Security: The Challenge of the Present. *Geoforum* **2018**, *91* (February), 73−77.

(3) *United Nations The Sustainable Development Goals Report 2019*; United Nations Publications, issued by Dep. Econ. Soc. Aff., 2019; p 64.

(4) Johnston, R. B. Arsenic and the 2030 Agenda for Sustainable Development. *Arsen. Res. Glob. Sustain. - Proc. 6th Int. Congr. Arsen. Environ. AS* **2016**, *2016*, 12−14.

(5) Beeckman, F.; Motte, H.; Beeckman, T. Nitrification in Agricultural Soils: Impact, Actors and Mitigation. *Curr. Opin. Biotechnol.* **2018**, *50*, 166−173.

(6) Mazzei, L.; Musiani, F.; Ciurli, S. The Structure-Based Reaction Mechanism of Urease, a Nickel Dependent Enzyme: Tale of a Long Debate. *JBIC, J. Biol. Inorg. Chem.* **2020**, *25* (6), 829−845.

(7) Van Kessel, M. A. H. J.; Speth, D. R.; Albertsen, M.; Nielsen, P. H.; Op Den Camp, H. J. M.; Kartal, B.; Jetten, M. S. M.; Lücker, S.

Complete Nitrification by a Single Microorganism. *Nature* **2015**, *528* (7583), 555−559.
(8) Norton, J. M.; Alzerreca, J. J.; Suwa, Y.; Klotz, M. G. Diversity of Ammonia Monooxygenase Operon in Autotrophic Ammonia-Oxidizing Bacteria. *Arch. Microbiol.* **2002**, *177* (2), 139−149.
(9) Arp, D. J.; Stein, L. Y. Metabolism of Inorganic N Compounds by Ammonia-Oxidizing Bacteria. *Crit. Rev. Biochem. Mol. Biol.* **2003**, *38* (6), 471−495.
(10) Maia, L. B.; Moura, J. J. G. How Biology Handles Nitrite. *Chem. Rev.* **2014**, *114* (10), 5273−5357.
(11) Coskun, D.; Britto, D. T.; Shi, W.; Kronzucker, H. J. Nitrogen Transformations in Modern Agriculture and the Role of Biological Nitrification Inhibition. *Nat. Plants* **2017**, *3* (June), 1−10.
(12) Timilsena, Y. P.; Adhikari, R.; Casey, P.; Muster, T.; Gill, H.; Adhikari, B. Enhanced Efficiency Fertilisers: A Review of Formulation and Nutrient Release Patterns. *J. Sci. Food Agric.* **2015**, *95* (6), 1131−1142.
(13) Cameron, K. C.; Di, H. J. The Use of a Nitrification Inhibitor, Dicyandiamide (DCD), to Decrease Nitrate Leaching and Nitrous Oxide Emissions in a Simulated Grazed and Irrigated Grassland. *Soil Use Manage.* **2002**, *18* (4), 395−403.
(14) Levett, I.; Pratt, S.; Donose, B. C.; Brackin, R.; Pratt, C.; Redding, M.; Laycock, B. Understanding the Mobilization of a Nitrification Inhibitor from Novel Slow Release Pellets, Fabricated through Extrusion Processing with PHBV Biopolymer. *J. Agric. Food Chem.* **2019**, *67* (9), 2449−2458.
(15) Gao, H.; Li, J.; Xu, F. Synthesis of a Novel Polymer Nitrification Inhibitor with Acrylic Acid and 3,4-Dimethylpyrazole. *J. Agric. Food Chem.* **2021**, *69* (11), 3307−3311.
(16) Musiani, F.; Broll, V.; Evangelisti, E.; Ciurli, S. The Model Structure of the Copper - Dependent Ammonia Monooxygenase. *JBIC, J. Biol. Inorg. Chem.* **2020**, *25* (7), 995−1007.
(17) (a) Wolt, J. D. Nitrapyrin Behavior in Soils and Environmental Considerations. *J. Environ. Qual.* **2000**, *29* (2), 367−379. (b) Vannelli, T.; Hooper, A. B. Oxidation of Nitrapyrin to 6-Chloropicolinic Acid by the Ammonia-Oxidizing Bacterium *Nitrosomonas europaea*. *Appl. Environ. Microbiol.* **1992**, *58*, 2321−2325. (c) Bremner, J. M.; Blackmer, A. M. Nitrous oxide: emission from soils during nitrification of fertilizer nitrogen. *Science* **1978**, *199*, 295−296.
(18) Ali, R.; Iqbal, J.; Tahir, G. R.; Mahmoood, T. Effect of 3,5-Dimethylpyrazole and Nitrapyrin on Nitrification under High Soil Temperature. *Pakistan J. Bot.* **2008**, *40* (3), 1053−1062.
(19) Goos, R. J. Evaluation of Two Products Recently Introduced as Nitrification Inhibitors. *Commun. Soil Sci. Plant Anal.* **2019**, *50* (5), 503−511.
(20) Woodward, E. E.; Edwards, T. M.; Givens, C. E.; Kolpin, D. W.; Hladik, M. L. Widespread Use of the Nitrification Inhibitor Nitrapyrin: Assessing Benefits and Costs to Agriculture, Ecosystems, and Environmental Health. *Environ. Sci. Technol.* **2021**, *55*, 1345.
(21) Casali, L.; Mazzei, L.; Shemchuk, O.; Honer, K.; Grepioni, F.; Ciurli, S.; Braga, D.; Baltrusaitis, J. Smart Urea Ionic Co-Crystals with Enhanced Urease Inhibition Activity for Improved Nitrogen Cycle Management. *Chem. Commun.* **2018**, *54* (55), 7637−7640.
(22) Casali, L.; Mazzei, L.; Shemchuk, O.; Sharma, L.; Honer, K.; Grepioni, F.; Ciurli, S.; Braga, D.; Baltrusaitis, J. Novel Dual-Action Plant Fertilizer and Urease Inhibitor: Urea·Catechol Cocrystal. Characterization and Environmental Reactivity. *ACS Sustainable Chem. Eng.* **2019**, *7* (2), 2852−2859.
(23) Mazzei, L.; Broll, V.; Casali, L.; Silva, M.; Braga, D.; Grepioni, F.; Baltrusaitis, J.; Ciurli, S. Multifunctional Urea Cocrystal with Combined Ureolysis and Nitrification Inhibiting Capabilities for Enhanced Nitrogen Management. *ACS Sustainable Chem. Eng.* **2019**, *7* (15), 13369−13378.
(24) Szejtli, J. Introduction and General Overview of Cyclodextrin Chemistry. *Chem. Rev.* **1998**, *98* (5), 1743−1753.
(25) Fernandes, J. A.; Ramos, A. I.; Ribeiro-Claro, P.; Almeida Paz, F. A.; Braga, S. S. Studies on Polymorph Conversion in a New Cyclodextrin Inclusion Compound. *CrystEngComm* **2015**, *17* (4), 937−946.
(26) Jansook, P.; Ogawa, N.; Loftsson, T. Cyclodextrins: Structure, Physicochemical Properties and Pharmaceutical Applications. *Int. J. Pharm.* **2018**, *535* (1−2), 272−284.
(27) Alsbaiee, A.; Smith, B. J.; Xiao, L.; Ling, Y.; Helbling, D. E.; Dichtel, W. R. Rapid Removal of Organic Micropollutants from Water by a Porous β-Cyclodextrin Polymer. *Nature* **2016**, *529* (7585), 190−194.
(28) López-De-Dicastillo, C.; Gallur, M.; Catalá, R.; Gavara, R.; Hernandez-Muñoz, P. Immobilization of β-Cyclodextrin in Ethylene-Vinyl Alcohol Copolymer for Active Food Packaging Applications. *J. Membr. Sci.* **2010**, *353* (1−2), 184−191.
(29) Gao, S.; Jiang, J.; Li, X.; Liu, Y.; Zhao, L.; Fu, Y.; Ye, F. Enhanced Physicochemical Properties and Herbicidal Activity of an Environment-Friendly Clathrate Formed by β-Cyclodextrin and Herbicide Cyanazine. *J. Mol. Liq.* **2020**, *305*, 112858.
(30) Smith, V. J.; Rougier, N. M.; de Rossi, R. H.; Caira, M. R.; Buján, E. I.; Fernández, M. A.; Bourne, S. A. Investigation of the Inclusion of the Herbicide Metobromuron in Native Cyclodextrins by Powder X-Ray Diffraction and Isothermal Titration Calorimetry. *Carbohydr. Res.* **2009**, *344* (17), 2388−2393.
(31) Geng, Q.; Xie, J.; Wang, X.; Cai, M.; Ma, H.; Ni, H. Preparation and Characterization of Butachlor/(2-Hydroxypropyl)-β-Cyclodextrin Inclusion Complex: Improve Soil Mobility and Herbicidal Activity and Decrease Fish Toxicity. *J. Agric. Food Chem.* **2018**, *66* (46), 12198−12205.
(32) Dos Santos Moreira, A. M.; Bittencourt, V. C. E.; Costa, F. L. S.; Elena De Lima, M.; Lopes, M. T. P.; Borges, W. S.; Martins, G. F.; Nascimento, C. S.; Da Silva, J. G.; Denadai, Â. M. L.; Borges, K. B. Hydrophobic Nanoprecipitates of β-Cyclodextrin/Avermectins Inclusion Compounds Reveal Insecticide Activity against Aedes Aegypti Larvae and Low Toxicity against Fibroblasts. *J. Agric. Food Chem.* **2018**, *66* (28), 7275−7285.
(33) Sheldrick, G. M. SHELXT - Integrated Space-Group and Crystal-Structure Determination. *Acta Crystallogr., Sect. A: Found. Adv.* **2015**, *71* (1), 3−8.
(34) Sheldrick, G. M. Crystal Structure Refinement with SHELXL. *Acta Crystallogr., Sect. C: Struct. Chem.* **2015**, *71* (Md), 3−8.
(35) MacRae, C. F.; Sovago, I.; Cottrell, S. J.; Galek, P. T. A.; McCabe, P.; Pidcock, E.; Platings, M.; Shields, G. P.; Stevens, J. S.; Towler, M.; Wood, P. A. Mercury 4.0: From Visualization to Analysis, Design and Prediction. *J. Appl. Crystallogr.* **2020**, *53*, 226−235.
(36) Coelho, A. A. *TOPAS-Academic V4.1*; Coelho Software: Brisbane, Australia, 2007.
(37) Hammersley, A. P.; Brown, K.; Burmeister, W.; Claustre, L.; Gonzalez, A.; McSweeney, S.; Mitchell, E.; Moy, J. P.; Svensson, S. O.; Thompson, A. W. Calibration and Application of an X-ray Image Intensifier/ Charge-Coupled Device Detector for Monochromatic. *J. Synchrotron Radiat.* **1997**, *4* (2), 67−77.
(38) Benecke, G.; Wagermaier, W.; Li, C.; Schwartzkopf, M.; Flucke, G.; Hoerth, R.; Zizak, I.; Burghammer, M.; Metwalli, E.; Müller-Buschbaum, P.; Trebbin, M.; Förster, S.; Paris, O.; Roth, S. V.; Fratzl, P. A Customizable Software for Fast Reduction and Analysis of Large X-Ray Scattering Data Sets: Applications of the New DPDAK Package to Small-Angle X-Ray Scattering and Grazing-Incidence Small-Angle X-Ray Scattering. *J. Appl. Crystallogr.* **2014**, *47* (5), 1797−1803.
(39) Gornall, A. G.; Bardawill, C. J.; David, M. M. Determination of Serum Proteins by Means of the Biuret Reaction. *J. Biol. Chem.* **1949**, *177* (2), 751−766.
(40) Griess, P. No Title. *Ber. Dtsch. Chem. Ges.* **1879**, *12*, 426−428.
(41) Mazzei, L.; Cianci, M.; Musiani, F.; Ciurli, S. Inactivation of Urease by 1,4-Benzoquinone: Chemistry at the Protein Surface. *Dalt. Trans.* **2016**, *45* (13), 5455−5459.
(42) James, S. L.; Adams, C. J.; Bolm, C.; Braga, D.; Collier, P.; Friščic, T.; Grepioni, F.; Harris, K. D. M.; Hyett, G.; Jones, W.; Krebs, A.; Mack, J.; Maini, L.; Orpen, A. G.; Parkin, I. P.; Shearouse, W. C.; Steed, J. W.; Waddell, D. C. Playing with Organic Radicals as Building Blocks for Functional Molecular Materials. *Chem. Soc. Rev.* **2012**, *41* (1), 413−447.

https://doi.org/10.1021/acs.cgd.1c00681
Cryst. Growth Des. 2021, 21, 5792−5799

(43) Do, J. L.; Friščić, T. Mechanochemistry: A Force of Synthesis. *ACS Cent. Sci.* **2017**, *3* (1), 13−19.
(44) Batzdorf, L.; Fischer, F.; Wilke, M.; Wenzel, K.-J.; Emmerling, F. Direct In Situ Investigation of Milling Reactions Using Combined X-Ray Diffraction and Raman Spectroscopy. *Angew. Chem.* **2015**, *127* (6), 1819−1822.
(45) Caira, M. R. On the Isostructurality of Cyclodextrin Inclusion Complexes and Its Practical Utility. *Rev. Roum. Chim.* **2001**, *46*, 371−386.
(46) Ramos, A. I.; Braga, T. M.; Silva, P.; Fernandes, J. A.; Ribeiro-Claro, P.; De Fátima Silva Lopes, M.; Paz, F. A. A.; Braga, S. S. Chloramphenicol·cyclodextrin Inclusion Compounds: Co-Dissolution and Mechanochemical Preparations and Antibacterial Action. *CrystEngComm* **2013**, *15* (15), 2822−2834.
(47) Rácz, C. P.; Borodi, G.; Pop, M. M.; Kacso, I.; Sánta, S.; Tomoaia-Cotisel, M. Structure of the Inclusion Complex of B-Cyclodextrin with Lipoic Acid from Laboratory Powder Diffraction Data. *Acta Crystallogr., Sect. B: Struct. Sci.* **2012**, *68* (2), 164−170.
(48) Mahalakshmi, G.; Balachandran, V. FT-IR, FT-Raman and DFT Study of 3,3′-Bis (Trifluoromethyl) Benzophenone and Its Biological Activity with Other Halogen (Cl, Br) Atoms. *Spectrochim. Acta, Part A* **2014**, *124*, 328−340.
(49) Sundaraganesan, N.; Ilakiamani, S.; Anand, B.; Saleem, H.; Joshua, B. D. FTIR, FT-Raman Spectra and Ab Initio DFT Vibrational Analysis of 2-Amino-5-Chloropyridine. *Spectrochim. Acta, Part A* **2006**, *64* (3), 586−594.
(50) D'Agostino, S.; Azzali, A.; Casali, L.; Taddei, P.; Grepioni, F. *ACS Sustainable Chem. Eng.* **2020**, *8* (35), 13215.
(51) Mohan, P. R. K.; Sreelakshmi, G.; Muraleedharan, C. V.; Joseph, R. Water Soluble Complexes of Curcumin with Cyclodextrins: Characterization by FT-Raman Spectroscopy. *Vib. Spectrosc.* **2012**, *62*, 77−84.
(52) Kumar, S.; Pooja; Trotta, F.; Rao, R. Encapsulation of Babchi Oil in Cyclodextrin-Based Nanosponges: Physicochemical Characterization, Photodegradation, and in Vitro Cytotoxicity Studies. *Pharmaceutics* **2018**, *10* (4), 169.
(53) Sardaru, M. C.; Carp, O.; Ursu, E. L.; Craciun, A. M.; Cojocaru, C.; Silion, M.; Kovalska, V.; Mangalagiu, I.; Danac, R.; Rotaru, A. Cyclodextrin Encapsulated PH Sensitive Dyes as Fluorescent Cellular Probes: Self-Aggregation and in Vitro Assessments. *Molecules* **2020**, *25* (19), 4397.
(54) Anaya-Castro, M. A.; Ayala-Zavala, J. F.; Muñoz-Castellanos, L.; Hernández-Ochoa, L.; Peydecastaing, J.; Durrieu, V. *β*-Cyclodextrin Inclusion Complexes Containing Clove (Eugenia Caryophyllata) and Mexican Oregano (Lippia Berlandieri) Essential Oils: Preparation, Physicochemical and Antimicrobial Characterization. *Food Packag. Shelf Life* **2017**, *14*, 96−101.
(55) Caira, M. R.; De Vries, E. J. C.; Nassimbeni, L. R. Crystallization of Two Forms of a Cyclodextrin Inclusion Complex Containing a Common Organic Guest. *Chem. Commun.* **2003**, *3* (16), 2058−2059.
(56) Byrne, M. P.; Tobin, J. T.; Forrestal, P. J.; Danaher, M.; Nkwonta, C. G.; Richards, K.; Cummins, E.; Hogan, S. A.; O'Callaghan, T. F. Urease and Nitrification Inhibitors-As Mitigation Tools for Greenhouse Gas Emissions in Sustainable Dairy Systems: A Review. *Sustainability* **2020**, *12* (15), 6018.

https://doi.org/10.1021/acs.cgd.1c00681
Cryst. Growth Des. 2021, 21, 5792−5799